Optical Properties of Antiferromagnetic Chromium and Dilute Cr-Mn and Cr-Re Alloys*

LAURENCE W. BOS† AND DAVID W. LYNCH
Institute for Atomic Research and Department of Physics, Iowa State University, Ames, Iowa 50010

(Received 11 May 1970)

The antiferromagnetic energy gap and optical properties of single crystals of Cr and of Cr alloyed with 0.45, 0.94, 2.5, and 4.5% Mn and with 1.05 and 2.0% Re have been investigated by measuring the optical absorption over a photon energy range of 0.08–5 eV. The data were taken at 4.2 K by a calorimetric technique. It is found that at 4.2 K, approximately 1% Mn or Re will cause commensurate antiferromagnetic ordering, and the energy gap shifts abruptly from 0.13 to 0.36 eV near this concentration of diluent. Evidence is given for indirect transitions occurring across a double energy gap in the noncommensurate samples, and the results are explained in terms of a band model. The widths of the absorption peak and the peak in ϵ_2 in the commensurate samples are discussed in terms of a gap anisotropy and impurity broadening. Optical absorption peaks near 1, 2, and 3.4 eV are associated with direct interband transitions originating from the N_1', Γ_{25}', and P_4 symmetry points, with a contribution to the 1-eV absorption from transitions from the Fermi surface to the flat unoccupied band extending through N_4, Γ_{12}, P_3, and H_{25}'.

INTRODUCTION

Chromium exhibits an interesting type of magnetic ordering which has been studied by a variety of techniques.[1] Anomalies appear in the transport properties as one passes through the Néel temperature[2,3] ($T_N=312$ K). A number of other physical properties change upon magnetic ordering. Neutron diffraction measurements have shown that the ordering is indeed antiferromagnetic[4] and that it does not have exactly twice the lattice periodicity that one would expect for a simple antiferromagnetic array of magnetic moments on lattice sites.[5] Below T_N the magnetization can be described by

$$\mathbf{M}(\mathbf{r})=\mathbf{M}_0\cos\mathbf{Q}\cdot\mathbf{r}, \tag{1}$$

where $\mathbf{Q}=(2\pi/a)(1-\delta,0,0)$. This differs from half the smallest [100] reciprocal-lattice vector $\mathbf{G}=(2\pi/a)\times(2,0,0)$ because of the small temperature-dependent term δ. δ varies from 0.05 at 4.2 K to 0.035 at T_N.[6–8] Above 123 K, $\mathbf{M}_0$ is perpendicular to $\mathbf{Q}$, while below 123 K, $\mathbf{M}_0$ is parallel to $\mathbf{Q}$.[7,8] The unusual periodicity of $\mathbf{M}(r)$, the fact that $\mathbf{M}$ can be parallel or perpendicular to $\mathbf{Q}$, and the fact that $|\mathbf{M}_0|$ corresponds to about 0.40 μ_B per Cr atom have led to the conclusion that spin-density waves (SDW) exist in Cr.[9] Thus chromium is an itinerant electron antiferromagnet, and one must consider its electronic band structure to understand the antiferromagnetism.

In a band model of itinerant magnetism one must consider two Fermi surfaces. For a ferromagnet, like iron, one surface would be for spin-up electrons, the other for spin-down. To establish a qualitative understanding of itinerant electron magnetism one assumes that the intra-atomic exchange (analogous to the Hund's rule energy for atomic orbitals) can be expressed in terms of a molecular field. As a result of the electronic spin's interaction with this field, an energy splitting occurs which leads to unequal populations in the spin-up and spin-down bands. For an itinerant antiferromagnet like Cr, one again thinks of two Fermi surfaces, one for electrons with spins in phase with the antiferromagnetism and the second for electrons with spins out of phase.

The existence of a SDW implies that the magnetic susceptibility $\chi(\mathbf{q},0)\rightarrow\infty$. The unenhanced magnetic susceptibility as given by perturbation theory is[10]

$$\chi^0(\mathbf{q})=N^{-1}\sum_{\mathbf{k},n,n'}[f_{\mathbf{k},n}(1-f_{\mathbf{k}+\mathbf{q},n'})/E_{n'}(\mathbf{k}+\mathbf{q})-E_n(\mathbf{k})], \tag{2}$$

where $f_{\mathbf{k},n}$ is the Fermi distribution function for the state $\mathbf{k}$ in band n, and $E_n(\mathbf{k})$ is the energy of an electron with wave vector $\mathbf{k}$ in band n. The above must be modified to take into account the exchange interaction $V(\mathbf{q})$, giving formally

$$\chi(\mathbf{q})=\chi^0(\mathbf{q})/[1-V(\mathbf{q})\chi^0(\mathbf{q})]. \tag{3}$$

The condition for a nonzero magnetic moment in the absence of an applied magnetic field is $V(\mathbf{q})\chi^0(\mathbf{q})=1$. Of course as $V\chi^0\rightarrow1$, the perturbation approach breaks down, but it is evident that whenever χ^0 tends to become large, an instability may result. An examination of Eq. (2) reveals that whenever there are two constant energy surfaces near the Fermi level having significant areas connected by some vector $\mathbf{q}$, $\chi^0(\mathbf{q})$ will become large.[11] $\chi(\mathbf{q})$ has been evaluated for Cr by Gupta and Sinha.[12]

A cross section of the Fermi surface of Cr [13] in the (100) plane is shown in Fig. 1. The important areas are the flat octahedral faces of the electron jack centered at Γ and the faces of the hole octahedron centered at H. As first pointed out by Lomer[11] these areas are responsible for the existence of the SDW in Cr. Figure 1 shows that two sides of the cross section of the hole octahedron are separated from the two sides of the cross section of the electron jack by the vector $\mathbf{Q}$ of

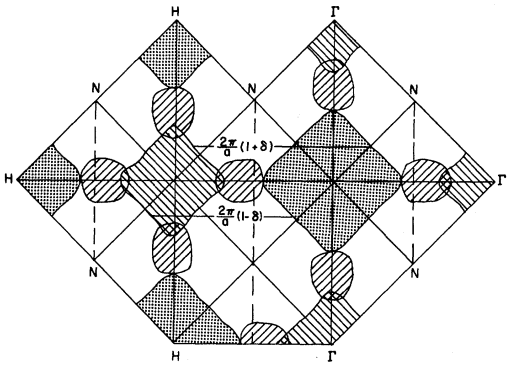

FIG. 1. Section in a (100) plane of the Fermi surface of Cr. The vector $\mathbf{Q}$ is shown, labeled $2\pi/a(1-\delta)$, as well as the vector $\mathbf{Q}=\mathbf{G}-\mathbf{Q}$, labeled $2\pi/a(1+\delta)$.

Eq. (1). States on, and near, these sections are strongly coupled and their energies displaced above and below the Fermi level. The electron jack is smaller than the hole octahedron, and differs somewhat in shape. As a result much, but not all, of the hole octahedron and central part of the electron jack are removed from the Fermi surface by the SDW. Figure 1 also shows the vector

$$\mathbf{Q}^*=\mathbf{G}-\mathbf{Q}=(2\pi/a)(1+\delta, 0, 0).$$

The periodic magnetization of Eq. (1) introduces a periodic term in the exchange potential, but one whose periodicity is not commensurate with that of the lattice. This introduces a series of gaps in the band structure. These gaps occur near, and are largest at, wave vectors $\mathbf{k}$ such that $E(\mathbf{k})=E(\mathbf{k}\pm n\mathbf{Q}\pm m\mathbf{G})$, where m and n are integers. The width of the $n=1$, $m=0$ gap, a "first-order" gap, is proportional to $|\mathbf{M}_0|$. Other gaps fall off fairly rapidly in width as n and m increase. An instructive model study of this phenomenon was carried out by Falicov and Zuckerman[14] and by Kimball.[15] The gap produced by $\mathbf{Q}^*$ (see Fig. 1) is a first-order gap in this picture, but the classification of gaps by order is somewhat model dependent.[14,15] In particular, some second-order gaps can be nearly as large as first-order gaps along particular lines in the Brillouin zone.[15] Moreover, $\mathbf{Q}$ can lie along any one of six equivalent [100] directions, but for a macroscopic single crystal, many domains usually form,[16] so that effectively all six equivalent $\mathbf{Q}$ vectors can be considered as introducing gaps in the band structure.

Figure 2 shows the band structure of paramagnetic Cr.[17] The bands of concern are Γ_{25}'-Σ_3-N_3, which goes through the center of the flat section of the electron jack (Fig. 1), and H_{25}'-G_3-N_2, which goes through the center of the flat section of the hole octahedron. These bands, where they cross the Fermi surface, are separated by $\mathbf{Q}$. Consequently they are split a considerable amount at the Fermi level, and lesser amounts away from it, by the part of the exchange potential proportional to $\cos\mathbf{Q}\cdot\mathbf{r}$. This is shown schematically in Fig. 3, where a splitting is also shown along the Δ direction, this splitting being smaller than on the flat parts of the Fermi surface because the electron jack and hole octahedron intersections with Δ are separated by a wave vector slightly different from $\mathbf{Q}$.

An optical transition is expected across such a gap,[18] because the wave functions for the states just below the gap have periodic factors $\cos(\frac{1}{2}\mathbf{Q}\cdot\mathbf{r})$ for spin-up and $\sin(\frac{1}{2}\mathbf{Q}\cdot\mathbf{r})$ for spin-down, while those for states just above the gap have factors $\sin(\frac{1}{2}\mathbf{Q}\cdot\mathbf{r})$ for spin-up and $\cos(\frac{1}{2}\mathbf{Q}\cdot\mathbf{r})$ for spin-down.[18] All other factors are essentially the same, so the electric dipole transition matrix element for a free-electron gas with a SDW is of the form

$$\int(\sin\tfrac{1}{2}\mathbf{Q}\cdot\mathbf{r})\,\mathbf{r}\,(\cos\tfrac{1}{2}\mathbf{Q}\cdot\mathbf{r})\,d^3r,$$

and does not vanish. No spin flip is necessary, and the transition occurs in all regions of the Brillouin zone near gaps.

Fedders and Martin[19] carried out a model calculation in which they obtain an expression for the "extra" optical absorption caused by transitions across the first-order gap. In their model, the electron jack and the hole octahedron are replaced by congruent spheres separated by a wave vector $\mathbf{Q}$. The attractive Coulomb interaction between electrons and holes connected by the wave vector $\mathbf{Q}$ creates bound electron-hole pairs in the triplet state. A mathematical analysis proceeds along the lines of the BCS theory of superconductivity, and the $T=0$ energy gap in this idealized model, at the Fermi surface, is given by $2\Delta=3.5kT_N$. This model predicts an optical conductivity whose real part is

$$\sigma_1(\omega)=\frac{4e^2k_F^2\Delta^2}{3\pi m\hbar\omega^2}\frac{\tanh(\hbar\omega/kT)}{[(\hbar\omega)^2-4\Delta^2]^{1/2}}. \qquad (4)$$

The inverse square-root singularity is, of course, nonphysical and arises from the isotropy of the electron-hole spheres and the lack of any type of scattering. Several optical studies have been made on Cr to determine the energy gap[20–22] and the prediction of the Fedders-Martin calculation is somewhat smaller than the 0.12 eV first observed.[21] Recent work[23] has been directed at quantitatively testing a version of the Fedders-Martin theory, modified to consider broadening caused by the electron-phonon interaction, with careful measurements of the temperature dependence of the infrared absorption peak in Cr. The electron-phonon interaction causes the gap energy to increase from its BCS value of $3.5kT_N=0.094$ eV to $5.1kT_N=0.137$ eV. It also removes the singularity in σ_1 at the gap energy. Kimball and Falicov[24] have investigated a two-band Hartree-Fock model and find the gap to be $4.3kT_N$, while Liu[25] has shown that imperfect nesting of electron and hole surfaces will cause the gap to exceed $3.5kT_N$.

Chromium-rich alloys with many solutes also exhibit antiferromagnetism. The Cr-Mn system has been studied extensively.[3,8] As Mn is added, T_N increases,

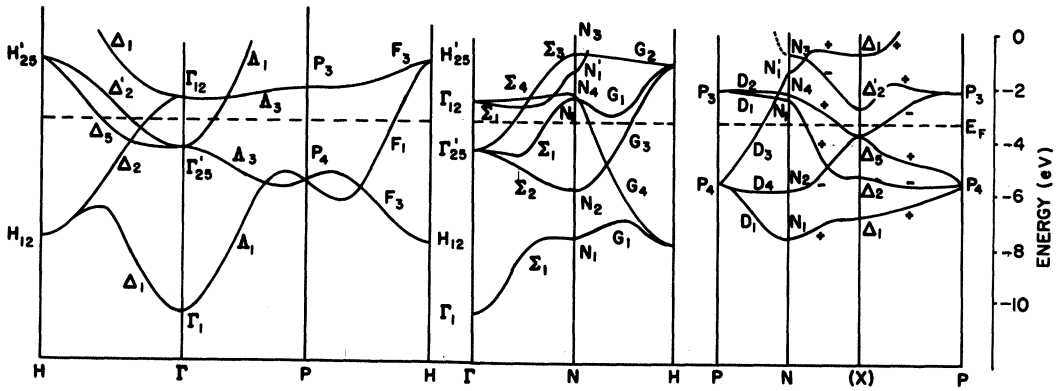

FIG. 2. Energy bands of paramagnetic Cr, after Asano and Yamashita, Ref. 17.

and the vector Q increases, i.e., δ decreases, until about 1% Mn has been added. At this point $\delta=0$ and it remains zero as more Mn is added.[8] This jump to commensurate ordering has been explained by Falicov and Penn[26] (see also Ref. 10). It can be understood qualitatively as an interplay between two energy-reducing mechanisms. One is due to the previously mentioned gaps in the energy bands which cross near the Fermi level, gaps arising from $\mathbf{M}(\mathbf{r})$ via the exchange potential. This raises the energy of empty states and reduces the energy of filled states. The value of Q that results is, as mentioned earlier, that which connects large areas of Fermi surface. As Mn is added, the electron concentration increases (see below), causing the electron jack to swell and the hole octahedron to shrink. Q thus grows with increasing Mn concentration, but is noncommensurate, since only at one Mn concentration will the large Fermi surface pieces be connected by a vector $|\mathbf{Q}|=2\pi/a$. However, there is a second effect, the intra-atomic Coulomb energy. This is minimized by having a larger moment at the ionic positions. After about 1% Mn is added, the latter effect becomes dominant and commensurate ordering results. The vector Q connecting the electron and hole Fermi surfaces continues to grow larger than $2\pi/a$ for increasing Mn concentration ($|\mathbf{Q}^*|$ in Fig. 1 then is smaller than $2\pi/a$), but itinerant electron exchange no longer dominates in the energy of magnetic ordering.

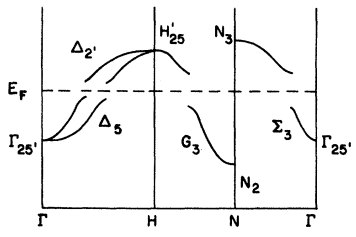

FIG. 3. Some first-order energy gaps introduced in the bands of Cr by a SDW.

Asano and Yamashita[17] have calculated the band structure of pure Cr in a hypothetical commensurately ordered state, a band structure which should be similar to that of the more concentrated Mn alloys.

According to the rigid-band theorem as applied to nearly free electrons, the effect of a perturbing potential due to the difference in valence between solute and solvent atoms is to shift every energy band without change of shape. However, the effect of the perturbation will, in general, be different for each band, which may cause the bands to shift relative to each other. The primary effect is to change the number of electrons/atom (e/a). This moves the Fermi level upward (downward) relative to the bottom of the band if a solute atom has more (less) valence electrons than a solvent atom.

It is not clear that this simple picture is applicable to the transition metals. The problem has been discussed in detail by Stern[27] and Beeby.[28] Stern has shown that when the parameter $\epsilon_{21}/\Delta\ll 1$, the alloy system has a single band structure which closely approximates that of a pure metal, and the rigid-band approximation is valid. Here ϵ_{21} is the magnitude of the difference of the atomic energies of the two constituents and Δ is the half-width of the band. The pure metal that is approximated is some average of the two constituents, and is well defined in the Cr-Mn system where the two elements, if placed in the same lattice, should have nearly the same band structure. Beeby has shown that the rigid-band model should be qualitatively correct for transition-metal alloys as long as the valence difference is small.

There is a considerable amount of experimental evidence tending to prove the validity of the rigid-band model for the Cr-Mn system. For example, neutron diffraction and electrical resistivity measurements on Cr-Mn-V ternary dilute alloys by Komura and Hamaguchi[29] show that there is a correspondence between effective Mn concentration and the magnetic moment and Néel temperature. Here the effective Mn concentration is defined as the Mn concentration minus the V

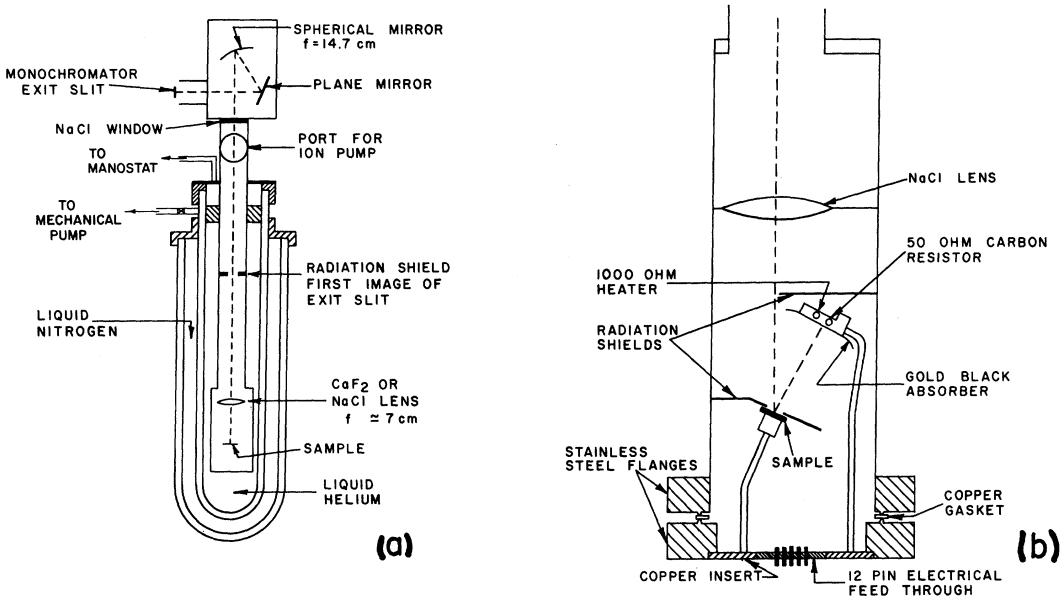

FIG. 4. Experimental arrangement: (a) general view, (b) sample and black absorber.

concentration in at. %. Thus at least for some physical quantities, the rigid-band model is of value in predicting results.

In this work, the optical properties of Cr alloyed with up to 4.5-at. % Mn (all compositions refer to at. %) and with up to 2% Re have been investigated over the energy range 0.1–5 eV by measuring the absorptivity at near normal incidence. One objective of this work was to examine the antiferromagnetic energy gap in Cr-Mn alloys and its relation to the theory of itinerant electron antiferromagnetism. In particular, the band gap was studied as a function of Mn concentration. A similar study has recently appeared[22,23] which is in substantial agreement with ours. Although the energy gap occurred in the infrared part of the spectrum, the absorptivity was also measured at higher photon energies so that a dispersion integral could be used to find the value of the phase of the amplitude reflection coefficients. The complex dielectric constant could then be calculated. These higher-energy data were also directly useful in helping locate the position of certain symmetry points in reciprocal space between which interband transitions occur. In particular, an absorbance peak near 1 eV was very sensitive to Mn or Re addition, and its origin could be identified. A preliminary account of our infrared data has already appeared.[30]

EXPERIMENTAL PROCEDURE

Instead of measuring the reflectivity R, we measured the absorptivity $A=1-R$ (for an opaque sample). In the infrared, R is high for metals, typically larger than 0.9, and to determine the height and shape of an interband transition in the infrared by measuring R is difficult because it appears as a small dip in R. If A is measured, the transition appears as a relatively large peak on a small background. Moreover, reflectivity measurements are difficult to make with high absolute accuracy.[31]

We used a calorimetric technique, originally used by Ramanathan[32] and by Pippard,[33] and more recently by others.[34–37] The arrangement is illustrated in Fig. 4. Monochromatic radiation from a prism double monochromator enters the cryostat and reaches the sample chamber. The sample and a gold-black-covered[38,39] copper absorber are thermally isolated from the 4.2-K walls of the chamber, except for thin copper heat-leak wires. The radiation, of intensity I_0, strikes, in turn, the sample and the black absorber which absorb energy at rates AI_0 and $(1-A)I_0$, respectively. (The gold-black absorbance was measured and found to be greater than 0.99 for $\lambda<12$ μ, falling to 0.98 at 14 μ.) The temperatures of the two "targets" then rise, with a time constant of 1–10s, and the steady-state temperatures are measured with carbon resistors. The radiation is then blocked off and the temperature rises of the two targets duplicated with resistance heaters. The input power to both heaters is then measured, and set equal to AI_0 and $(1-A)I_0$, from which A can be found. By using a variety of prisms and light sources, the wavelength range 0.24–14.0 μ could be spanned, with the incident power I_0 exceeding 10 μW for acceptable spectral bandpass. Near 2 μ, up to 150 μW could be directed on the sample using a bandpass of 0.1 μ. The absorber was large enough to collect a fraction of any nonspecularly reflected radiation from the sample, reducing errors due to nonflat sample surfaces.

The accuracy of the measurements is directly related

to the amount of energy incident upon the sample. Since the energy available is smallest in the infrared, the accuracy suffered somewhat at wavelengths beyond 6 μ. At 10 μ, with an absorptivity of 0.050, the temperature change for 1 μW of power absorbed by the sample was typically about 0.007 K, and could be reproduced to within 2%, leading to a 2% uncertainty in A. This means the absorptivity was 0.050 ± 0.001, neglecting other sources of error. Comparable accuracy would require R to be measured as 0.950 ± 0.001. A considerable increase in sensitivity resulted from pumping on the liquid-helium bath, but there was some loss of stability.

All data were taken at an average angle of incidence of 15°. If the incident radiation were s- or p-polarized, an appreciable correction, one requiring knowledge of the optical constants of the sample, would be necessary to obtain the normal-incidence absorptivity. However, the output of the monochromator and subsequent optical elements was only slightly polarized, so the correction for non-normal incidence was negligible.

This method is not without its disadvantages. Relatively large amounts of power are needed, requiring a large spectral bandpass. The resolution was more than adequate for the present work, and probably is adequate for all work on metals. All measurements must be made at, or near, liquid-helium temperature (so that heat capacities are small) so that the temperature dependence[23] cannot be studied.

Sample Preparation

All samples were cut from single-crystal ingots grown by arc-zone melting.[40] The ingots were 8 cm long with a cross section of 1 cm^2. Often almost the entire ingot could be made into a single crystal. The Cr was estimated to be 99.999% pure and the Mn 99.97% pure. Two samples were spark-cut from the lower portion of each ingot. The lowermost portion was used for a composition analysis by flame-emission spectroscopy, while the lower surface of the adjacent piece was used for optical measurements. After etching in a solution of boiling HCl, the surface was ground and polished using 4/0 emery paper followed by 1- and 0.3-μ aluminum oxide abrasive. The surface was then electropolished using a 6% solution of perchloric acid in methyl alcohol at −78°C. The crystal was annealed at 1150°C for 2 h inside a Ta tube filled with Ar. The sample was then electropolished a second time, rinsed in absolute methyl alcohol, and mounted in the sample chamber. The Cr-Mn samples used contained about half the Mn concentrations of the starting material, due to the much higher vapor pressure of Mn during the melting processes. The final arc-melting step which forms the single crystal was particularly effective in vaporizing Mn from the crystal. An electron microprobe analysis indicated that in the upper 2 or 3 mm of the crystal, virtually no Mn remained. The boundary between these two regions could be seen easily by strongly etching a cross section of the ingot.

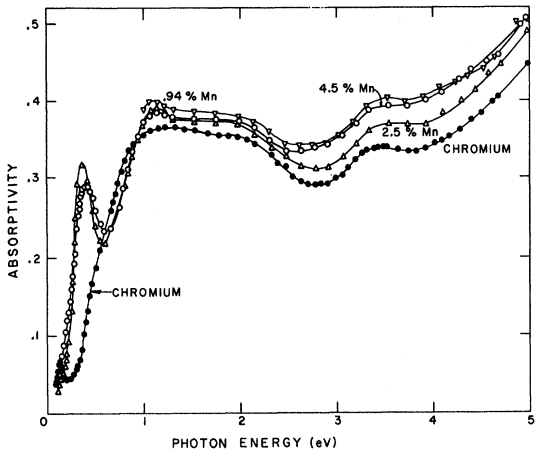

FIG. 5. Absorptivity spectra of Cr and several Cr-Mn alloys, showing antiferromagnetic absorptivity peaks and interband absorption structure.

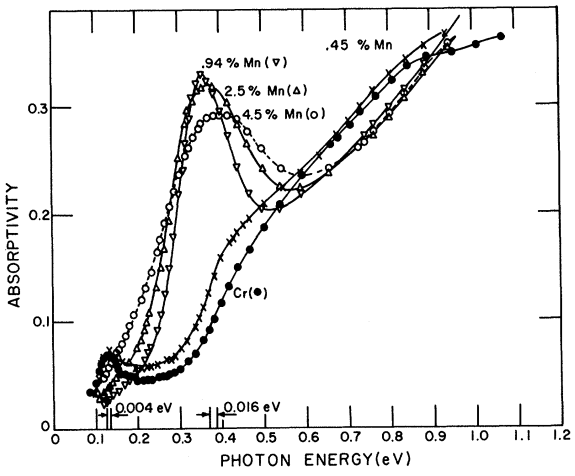

FIG. 6. Absorptivity spectra of Cr and several Cr-Mn alloys, showing the movement of the antiferromagnetic peak as Mn is added. The spectral bandpass is indicated by arrows.

EXPERIMENTAL RESULTS

The curves of absorptivity versus photon energy are shown in Figs. 5–8. All data at photon energies below 0.12 eV were taken at 3.5 K instead of 4.2 K. No discontinuity could be observed due to the temperature difference. The peaks at about 0.13 and 0.38 eV are due to transitions across the gaps introduced by the SDW. Reference 23 discusses other possible causes of these peaks and shows they are unlikely.

There do not exist extensive reflectivity data on pure Cr in the visible and ultraviolet, even at room temperature.[41,42] In the infrared, one can compare our results with those of Hughes and Lawson[20] on a poly-

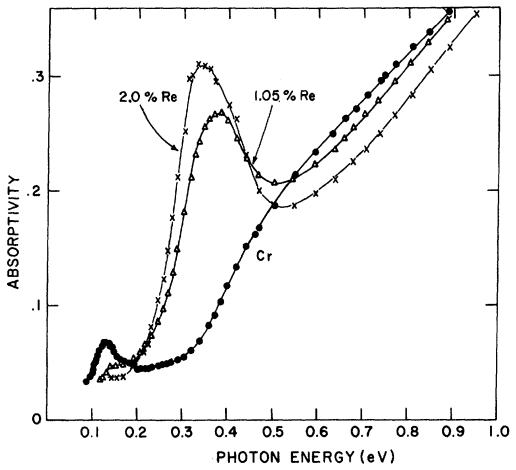

FIG. 7. Absorptivity spectra of Cr and two Cr-Re alloys.

crystalline sample at 107 K and those of Barker and co-workers[21–23] on a single crystal at 80 K. This is shown in Fig. 8 and the agreement is only fair, even considering the temperature difference (Ref. 21 indicates little difference between their results at 80 and at 20 K). In particular, there is disagreement in the location of the reflectivity minimum due to the gap introduced by noncommensurate ordering. Our gap is higher in pure Cr. The reason for this is unknown. Preliminary reflectivity measurements[43] (using other apparatus) give a reflectivity dip more in agreement with our results.

To extract more information from the absorptivity data requires the use of a dispersion integral or Kramers-Kronig integral. The magnitude of the complex amplitude reflection coefficient $\tilde{r}$ can be used[44,45] in such an integral to get α, the phase of $\tilde{r}$,

$$\alpha(\omega_0)=\frac{2\omega_0}{\pi}P\int_0^\infty \frac{\ln|\tilde{r}|}{\omega_0^2-\omega^2}\,d\omega, \tag{5}$$

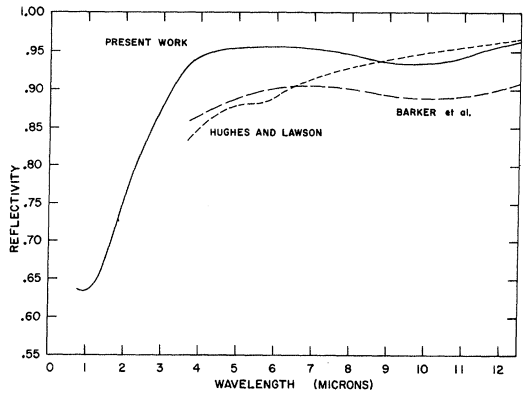

FIG. 8. Comparison of the reflectivity of Cr measured in the present work at 4.2 K with previous results at 80 K (Refs. 20 and 21).

where $|\tilde{r}|^2=1-A$ and the P signifies principal value. To calculate the phase at a frequency ω_0 requires, in principle, a knowledge of $|\tilde{r}|$ everywhere. However, the largest contribution to the integral originates in the frequency region around ω_0, and an extrapolation procedure can often be used to approximate the reflectivity at very high energies. The upper limit of the present data is 5 eV, and for 5 eV$<E<$30 eV, the data of Girault *et al.*[46] were used. Above 30 eV, the reflectivity was assumed to be of the form $R=R_2\exp[B(E_2-E)]$, where R_2 is the reflectivity at the energy E_2, the maximum energy for which data are available. B was chosen to give a continuous derivative of the reflectivity at R_2.

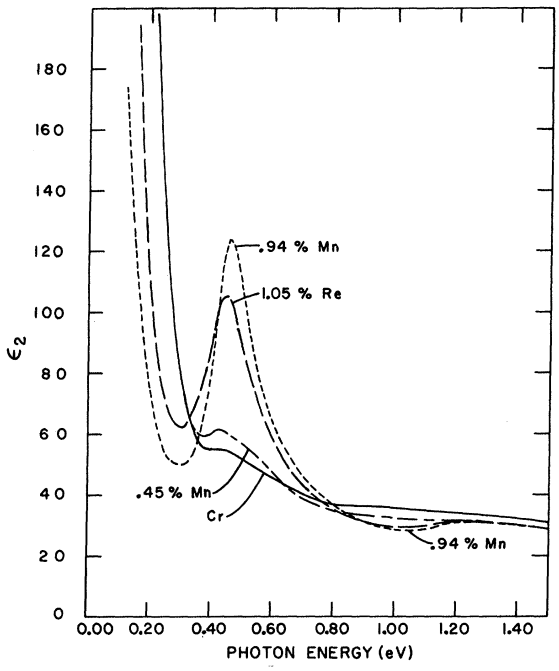

FIG. 9. Imaginary part of the dielectric constant of Cr and several Cr alloys, obtained from Kramers-Kronig analysis of the absorptivity spectra.

The integral was terminated at an energy E_3 to allow convergence and give good agreement in the region from 5 to 10 eV with the data of Girault *et al.* It should be pointed out that the use of such an extrapolation is not fundamentally sound and can lead to serious errors if attempts are not made to insure accurate optical constants at some point in the region where reflectivity data are available. Although changing E_3 caused relatively slight variations in ϵ_1 and ϵ_2 below 1 eV, above this energy appreciable modifications in $\tilde{\epsilon}$ occurred. Hence, the ϵ_1 and ϵ_2 curves for 1 eV$<E<$4 eV should not be trusted for absolute accuracy. These curves have the correct shape but may be displaced vertically from their true values. After the phase had been found, the complex dielectric function was obtained from the rela-

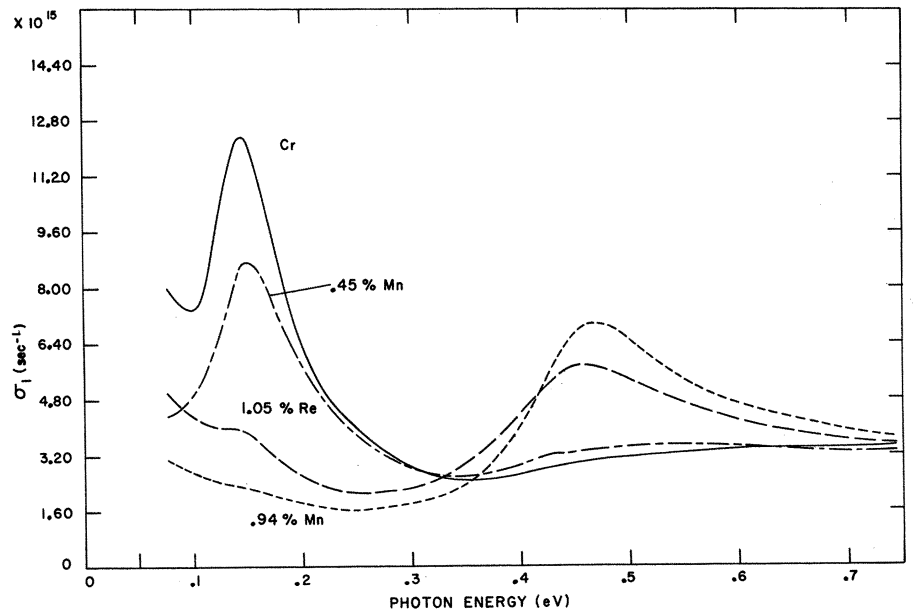

FIG. 10. Real part of the conductivity for two commensurate and two noncommensurate samples.

tions

$$n=(1-R)/(1+R-2R^{1/2}\cos\alpha), \quad (6)$$

$$k=2R^{1/2}\sin\alpha/(1+R-2R^{1/2}\cos\alpha), \quad (7)$$

$$\epsilon_1=n^2-k^2, \quad (8)$$

$$\epsilon_2=2nk. \quad (9)$$

Figures 9 and 10 illustrate the calculated values of ϵ_2 and $\omega\epsilon_2/4\pi=\sigma_1$, the real part of the complex conductivity. For pure Cr, with a resistivity ratio of 200, ϵ_2 and σ_1 are not correct. At 4 K the mean free path of the free electrons is larger than the characteristic penetration depth of the light, and the theory of the anomalous skin effect must be used. A local (**k**-independent) dielectric constant or conductivity does not exist. The interband contributions to ϵ_2 and σ_1 are probably close to correct in Figs. 9 and 10, however, for the peak at 0.13 eV is similar to that in Cr+0.45% Mn, where the anomalous skin effect is truly negligible. Thus the only incorrect parts of Figs. 9 and 10 are the parts representative of the free-electron gas for pure Cr, and they should not be greatly in error.

TABLE I. Location and size of the antiferromagnetic absorption peak.

Sample	Energy of peak absorptivity (eV)	Peak absorptivity	Gap edge (eV)
Chromium	0.13	0.068	0.08
Cr-0.45% Mn	0.135	0.074	0.08
Cr-0.94% Mn	0.36	0.331	0.20
Cr-2.5% Mn	0.37	0.320	0.14
Cr-4.5% Mn	0.40	0.292	0.10
Cr-1.05% Re	0.38	0.268	0.20
Cr-2.0% Re	0.36	0.310	0.17

DISCUSSION

Concentration Dependence of Gap Energy

From Fig. 6, the absorptivity peaks are seen to be near 0.13 or 0.38 eV. Table I illustrates the effect of alloy concentration on the magnitude and location of the energy gap (see also Ref. 23). Also listed is the gap edge, i.e., the least energy necessary to cause the absorption to increase above the free-electron background as determined by examining the low-energy side of the absorptivity peak. The most noticeable feature of these data is the abrupt change in size and location of the absorptivity peak that occurs between 0.45 and 0.94% Mn. It is between these concentration limits that the antiferromagnetism changes from the noncommensurate to the commensurate structure.

Noncommensurate Antiferromagnetism

Fermi-Surface Properties

The band picture, in this case, has been discussed in the Introduction. If $|\mathbf{Q}|/|\mathbf{G}|$ is not a rational number, the reduced zone scheme is no longer valid although the concept remains useful. A great many energy gaps appear in the one-dimensional dispersion rela-

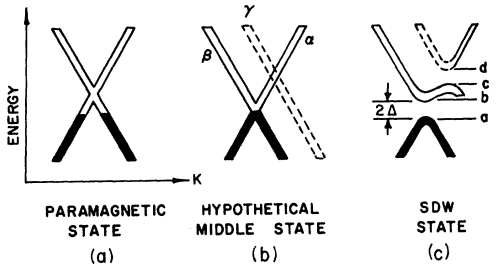

FIG. 11. Simplified band structure showing middle state and double energy gap, after Ref. 17. In (a) the band with positive slope (α) is, for example, Σ_3 and the band with negative slope (β) is G_3, displaced a distance Q to the left of its original position. In (b) another G_3 band (γ) has been drawn after having been displaced by Q* to the right of its original position. (c) shows the bands of (b) after the SDW is "turned" on. The black parts of the bands are filled.

tion, and the size of these gaps has been discussed by several authors.[14,15,26]

The gap dependence on Mn or Re concentration can be understood by referring to the energy bands for paramagnetic Cr (Fig. 2) and the Fermi-surface cross section (Fig. 1). The band calculations are due to Gupta,[47] who used the augmented-plane-wave (APW) method, and Asano and Yamashita,[17] who used the Green's-function technique. As one increases the Mn content, the e/a ratio increases, thus raising the Fermi energy. The electron surface at Γ increases in size, the hole surface at H decreases in size, and both effects cause Q, the superlattice vector, to get larger. With increased Mn, the average magnetic moment and Néel temperature are observed to increase,[8] implying a stronger exchange interaction. This is likely to be due to larger areas of the Fermi surface being coupled by the Q vector. As $\delta \rightarrow 0$ all four flat sides of the electron jack are coupled to sides of the hole octahedron. Since the gap energy is proportional to $|\mathbf{M}_0|$, the amplitude of the SDW, one expects an increase in the gap energy as Mn is added. By comparing the results of the Cr and Cr-0.45% Mn samples, the gap energy is seen to increase slightly in accord with the above prediction. This can also be seen in Refs. 22 and 23.

Evidence for Indirect Transitions across Two Energy Gaps

The complex dielectric constant (especially ϵ_2) reveals information about the types of transitions that are occurring near the gap energy. The Cr-0.45% Mn absorption peak occurs near where the peak occurs in pure Cr and the conductivities are similar. Yet ϵ_2 exhibits a slight bump at approximately 0.4 eV, where the commensurate samples have a large ϵ_2 peak (Fig. 9). This could have two origins: (i) crystal inhomogeneities, or (ii) indirect transitions across two energy gaps.

It is possible that small regions exist in the crystal which have a locally higher Mn concentration. If such a region were the size of one of the antiferromagnetic domains which make up an annealed crystal, it would be large enough to support a commensurate SDW. The size of these domains is not known, but neutron diffraction results indicate cubic symmetry in non-field-cooled samples,[8] which implies a domain size small compared with the dimensions of the neutron beam, i.e., a fraction of a mm. Actually, much smaller regions probably could exist as antiferromagnetic domains.

To explore the second possibility, consider a section of the band structure as shown in Fig. 11. The energy gaps are those due to Q and to Q*. Energy gaps can be found by displacing paramagnetic bands by Q in k space. Whenever two such displaced bands cross at the Fermi level, gaps will appear. The plane of Fig. 11 is perpendicular to the (100) plane of Fig. 1, and it contains the vector Q shown there. Thus it runs parallel to the [100] direction, but cuts the hole octahedron, and central part of the jack, missing the balls on the jack. In Fig. 11(a) the band rising toward the right passes through the flat face of the electron jack at the Fermi surface. The other band passes through a hole octahedron to the right of the jack, but it has been displaced to the left by Q. Figure 11(b) now brings in another band passing through another hole octahedron, one originally to the left of the electron jack. This band was displaced by Q* to the right to appear in Fig. 11(b). Figure 11(c) shows these bands after the interaction has split them. An indirect transition between a and d would require an energy close to the commensurate gap energy and a momentum change of $\hbar\,|\,\mathbf{Q}^*-\mathbf{Q}\,|=4\pi\hbar\delta/a$. The lack of momentum conservation might be explained by impurity or phonon scattering, but it is not necessary. Kimball[15] has shown that in a noncommensurate antiferromagnet allowed optical transitions occur in which k changes by Q or Q*. This effect may also occur in the pure Cr sample, as evidenced by the shoulder in ϵ_2 near 0.4 eV. Such a

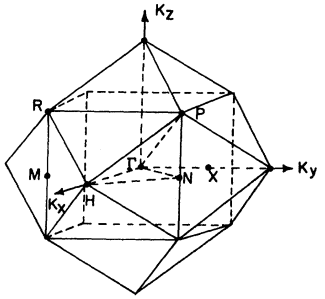

FIG. 12. Brillouin zones for the bcc space lattice (that of paramagnetic Cr) and the simple cubic space lattice (that of commensurately ordered Cr alloys). States within the pyramidal volume described by the plane containing N and P perpendicular to the k_y axis and the point H on the k_y axis are remapped into the equivalent volume within the cubic zone described by the plane containing M and R perpendicular to the k_y axis and the point Γ.

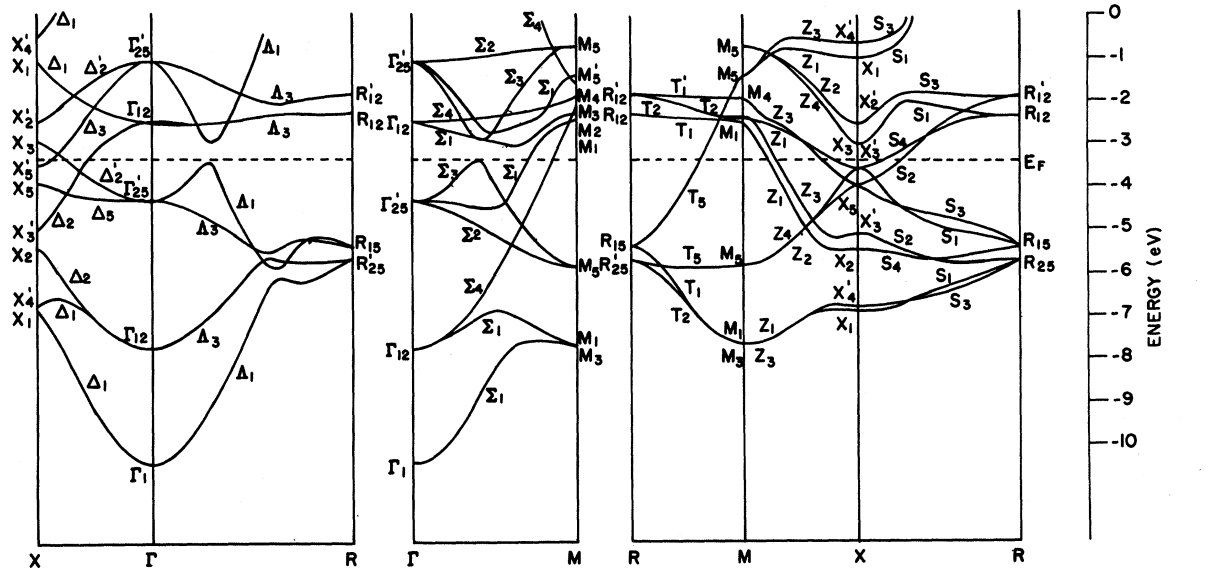

FIG. 13. Energy bands for hypothetical commensurately antiferromagnetically ordered Cr, after Ref. 17. The bands of Fig. 2 are remapped into the simple cubic zone (Fig. 12), and degeneracies at the new zone boundaries lifted by the crystal potential. The bands from H to P in Fig. 2 are now from Γ to R, and the Γ-Δ-H bands are now Γ-Δ-X-Δ-Γ. The antiferromagnetic gaps are along Δ and Σ.

shoulder should not be due to commensurate-phase regions in the sample, unless they can occur without appreciable impurities. One expects a weaker effect in pure Cr because more momentum is required for the indirect transition (δ is larger than in the 0.45% alloy) and possibly because there is less scattering to supply the momentum. Even if we are observing both phases in the Cr-0.45% Mn sample, the fact that the absorptivity of the commensurate samples is less than the absorptivity of the noncommensurate samples at photon energies between 0.6 and 0.9 eV is still unexplained (Figs. 6, 7, and 9), unless indirect transitions occur in the noncommensurate samples in this energy range as discussed above. They would not occur in the commensurate samples.

Commensurate Antiferromagnetism

Commensurate Antiferromagnetic Energy Gap in Band Picture

The sudden increase in gap energy for the 0.94% Mn sample can be attributed to achieving commensurate ordering. Falicov and Penn[26] have considered a model where the energy gaps caused by $\mathbf{Q}$ and $\mathbf{Q}^*$ merge together as $|\mathbf{Q}| \rightarrow 2\pi/a$ (i.e., $\delta \rightarrow 0$), and the commensurate structure is reached. This model predicts a gap which is larger by a factor of 2 than the gap in noncommensurate antiferromagnetism (Fig. 11). Experimentally, this is not very different from the results obtained by optical absorption.

When the commensurate structure is reached, the magnetic ordering is essentially that of a simple antiferromagnet. The Brillouin zone for the bcc structure must be replaced by a new zone, the magnetic superzone, which is cubic and has one-half the volume of the bcc Brillouin zone (Fig. 12).

In going from the paramagnetic to the antiferromagnetic case, the Fermi surface and energy bands undergo certain alterations. The bands of Fig. 2 can be remapped, and the self-consistent interaction causes the bands to split, forming an energy gap at the superzone boundary (Fig. 13). However, far more important is the energy gap which appears due to the accidental degeneracy as can be seen on the Λ and Σ axes near the Fermi level. A considerable portion of the Fermi surface is annihilated, and the resulting gap is responsible for the large absorption peak near 0.36 eV in the commensurate samples.

Asano and Yamashita[17] have also calculated the band structure of a hypothetical commensurate Cr using the Green's-function method (Fig. 13). They represented the exchange interaction by an adjustable parameter λ, determined so as to give a spin polarization of 0.6 μ_B per atom. They determined the energy gap along the Λ and Σ axes to be 0.4 eV, which is in good agreement with the optical measurements observed here.

Gap Anisotropy

The area under the ϵ_2 curve, $\int \epsilon_2(E)\,dE$, in the vicinity of the gap energy should be proportional to the amount of Fermi surface annihilated by the magnetic ordering. This is because the annihilated states are bunched together at either side of the gap and it is between these states that the transitions occur. According to a band-

structure calculation[17] done on hypothetical commensurate Cr, the density of states at the Fermi energy is reduced by about 29%. Energy-band calculations indicate that the energy gap, which can be seen on the Λ and Σ axes, exists in almost all directions from Γ. Practically the entire electron surface around Γ and the hole surface at H are eliminated by the magnetic ordering. As can be seen from Fig. 13, there is no gap on the Δ axis, and the hole pockets remain around N. A small gap is indicated in Fig. 3, but when the electron jack swells and the hole octahedron shrinks, this gap becomes smaller.

The width of the absorption peak measured on the 0.94% Mn crystal is about 0.14 eV, and considering that the data were taken at 4.2 K, it is apparent that some form of broadening other than phonon broadening is occurring. Some impurity scattering is surely present, but it is also possible that anisotropies in the gap energy are responsible for this effect. Although the band calculations indicate almost the same gap energy along the Λ and Σ axes, near the Δ axis the energy gap will be smaller. This may be the reason for the appreciable absorption that occurs at energies as low as 0.2 eV in the commensurate alloys. There will also be a smearing out of the absorption peak due to impurity scattering. The larger width of the absorption peak at higher Mn concentrations can be attributed to increased impurity scattering and possibly to a larger gap anisotropy. The energy of peak absorption increases with increasing Mn content, in agreement with neutron diffraction measurements which indicate a larger moment as Mn is added.

Conductivity Function and Evidence for Mixed Phase

The conductivities of the commensurate samples exhibit the same broad structure observed in the absorption spectra. Two representative curves are shown in Fig. 10. One of these is a Cr-1.05% Re sample run for comparison purposes. Re is in the same column of the Periodic Table as Mn and should increase e/a as does Mn. However, the Re ion is much larger and will have other effects such as an expansion of the lattice and a less similar potential at the lattice site. It is interesting to note that at $T\approx 0$ the commensurate phase is reached with the addition of about 1% Re just as with Mn.

The Cr-1.05% Re sample exhibits a smaller ϵ_2 peak near 0.4 eV compared to the commensurate samples (Fig. 7). Also, the conductivity and absorptivity curves give weak indication of noncommensurate behavior near 0.15 eV. This effect is believed due to crystal inhomogeneities since the composition lies near the phase boundary.[48]

Higher-Energy Interband Transitions

The interband spectra are difficult to analyze, because (a) many bands occur having states with energies near E_F and (b) band calculations made by different authors are not in complete agreement.

To determine what transitions are likely to occur requires finding the occupied states $|i\rangle$ and unoccupied states $|f\rangle$ for which the matrix element, proportional to $\langle f|\hat{n}\cdot\mathbf{p}|i\rangle$ or $\langle f|\hat{n}\cdot\mathbf{r}|i\rangle$, does not vanish. $\hat{n}$ is a unit vector in the direction of polarization of the incident radiation, and $\mathbf{p}$ and $\mathbf{r}$ are electron momentum and position operators, respectively. By using group theory, one can determine if the latter dipole matrix element is nonzero. Required is a decomposition of the direct product $\Gamma_r\times\Gamma_i$ to see if it contains the irreducible representation Γ_f. Here Γ_i (Γ_f) is the irreducible representation of the initial (final) state, and Γ_r is the irreducible representation of the operator x, y, or z. Sachs[49] has tabulated selection rules for many direct optical transitions involving Bloch functions with $\mathbf{k}$ vectors along symmetry lines. We have used these and calculated a few others, using character tables.[50,51] All the transitions to be mentioned are electric-dipole allowed.

The first strong interband absorption peak is near 1 eV (Fig. 5). Except for superzone gaps at X, in commensurate samples only, the only symmetry point where this transition might occur is at N, namely, the $N_1'\rightarrow N_1$, $N_1'\rightarrow N_4$ complex. According to the calculations of Loucks[13] and Gupta,[47] the Fermi level occurs very near N_1', and they cannot predict with certainty that a hole pocket exists there. The calculations of Asano and Yamashita[17] show definitely the existence of a hole pocket at N_1'. Graebner and Marcus[52] find a small hole pocket at N by de Haas–van Alphen effect measurements on antiferromagnetic Cr. Assuming the existence of a small hole pocket at N_1', alloying with Mn would tend to enhance this transition due to filling the bands denoted by G_4 and Σ_1. When they are filled, the transition would occur at a critical point in the joint density of states. Since an enhancement does occur, we associate the $N_1'\rightarrow N_1$, $N_1'\rightarrow N_4$ complex with the peaked part of the broad absorption near 1 eV. It should be pointed out that if Asano's calculations are correct, our analysis would not be valid since then the point N_1' lies 0.8 eV above the Fermi level. Then the Σ_1 band near N would intersect the Fermi surface at a large angle, and the density of states would increase only slowly with additional Mn. Under these conditions the Σ_1 band at N would not be populated (unless large quantities of Mn were added) and no enhancement would be expected. In either case, a large part of the edge at 1 eV (but not the increase in absorption that occurs upon alloying) should be attributed to transitions between the Fermi surface and the flat band $\Gamma_{12}\rightarrow P_3\rightarrow N_1$, $N_4\rightarrow H_{25}'$ (Fig. 2). There exists an appreciable volume in $\mathbf{k}$ space where transitions to this band from the Fermi surface can occur. A similar situation exists in copper.[53] It is possible that both processes contribute to the 1-eV peak.

The shoulder near 2 eV can be associated with the $\Gamma_{25}'\rightarrow\Gamma_{12}$ transition. Both band calculations list the energy difference as being about 1.85 eV.

The peak near 3.4 eV is probably the $P_4\rightarrow P_3$ of

Gupta's calculation (4 eV) or the corresponding $R_{15}\rightarrow R_{12}$ (3.1 eV) of Asano. A gradual increase in absorbance begins at 4 eV and continues to the limit of the data. (The data of Girault *et al.*[46] indicate the peak occurs at about 5.5 eV.) It should be reiterated that band-structure curves are very sensitive to the potential used in their calculation, and it is possible that later calculations will prove our associations incorrect. However, there does seem to be a good correspondence between the band calculations and our optical measurements.

Note added in proof. The statements made above on the filling of hole pockets at N and the associated enhancement of the absorption are not consistent with preliminary interpretation of de Haas–van Alphen data on Cr-Mn alloys [E. Gutman (private communication)]; the signal identified as arising from hole pockets at N indicates these pockets become larger in cross section as Mn is added, not smaller as we have inferred.

ACKNOWLEDGMENTS

Several people contributed significantly to this work. F. A. Schmidt prepared all of the ingots and annealed all the samples, and C. C. Butler performed the analyses of their compositions. We wish to acknowledge their contributions. Discussions with Dr. R. P. Gupta and Professor J. L. Stanford were beneficial.

* Work performed in the Ames Laboratory of the U.S. Atomic Energy Commission. Contribution No. 2722.

† Present address: Western Electric Co., Engineering Research Center, Box 900, Princeton, N.J. 08540.

[1] A. Arrott, in *Magnetism*, edited by G. T. Rado and H. Suhl (Academic, New York, 1966), Vol. IIB, p. 276.
[2] H. H. Potter, Proc. Phys. Soc. (London) **53,** 695 (1941).
[3] A. L. Trego and A. R. Mackintosh, Phys. Rev. **166,** 495 (1968).
[4] C. G. Shull and M. K. Wilkinson, Rev. Mod. Phys. **25,** 100 (1953).
[5] L. Corliss, J. Hastings, and R. Weiss, Phys. Rev. Letters **3,** 211 (1959).
[6] G. E. Bacon, Acta Cryst. **14,** 823 (1961).
[7] G. Shirane and W. J. Takei, J. Phys. Soc. Japan Suppl. **17,** 35 (1962).
[8] W. C. Koehler, R. M. Moon, A. L. Trego, and A. R. Mackintosh, Phys. Rev. **151,** 405 (1966).
[9] A. W. Overhauser, Phys. Rev. **128,** 1437 (1962).
[10] C. Herring, in Ref. 1, Vol. IV, especially Chaps. III, XII, and XIII.
[11] W. M. Lomer, Proc. Phys. Soc. (London) **84,** 489 (1962).
[12] R. P. Gupta and S. K. Sinka, J. Appl. Phys. **41,** 915 (1970).
[13] T. L. Loucks, Phys. Rev. **139,** A1181 (1965).
[14] L. M. Falicov and M. J. Zuckerman, Phys. Rev. **160,** 372 (1967).
[15] J. C. Kimball, Phys. Rev. **183,** 533 (1969).
[16] J. E. Graebner and J. E. Marcus, J. Appl. Phys. **37,** 1262 (1966).
[17] S. Asano and J. Yamashita, J. Phys. Soc. Japan **23,** 714 (1967).
[18] A. W. Overhauser, Phys. Rev. Letters **13,** 190 (1964); but see also J. J. Hopfield, Phys. Rev. **139,** A419 (1965).
[19] P. A. Fedders and P. C. Martin, Phys. Rev. **143,** 245 (1966).
[20] R. S. Hughes and A. W. Lawson, Phys. Letters **25A,** 473 (1967).
[21] A. S. Barker, B. J. Halperin, and T. M. Rice, Phys. Rev. Letters **20,** 384 (1968).
[22] T. M. Rice, A. S. Barker, B. I. Halperin, and D. B. McWhan, J. Appl. Phys. **40,** 1337 (1969).
[23] A. S. Barker and J. A. Ditzenberger, Phys. Rev. B **1,** 4378 (1970).
[24] J. C. Kimball and L. M. Falicov, Phys. Rev. Letters **20,** 1164 (1968).
[25] S. H. Liu, Phys. Letters **27A,** 493 (1968).
[26] L. M. Falicov and D. R. Penn, Phys. Rev. **158,** 476 (1967).
[27] E. A. Stern, Physics **1,** 255 (1965).
[28] J. L. Beeby, Phys. Rev. **135,** A130 (1964).
[29] S. Komura and Y. Hamaguchi, J. Phys. Soc. Japan **23,** 171 (1967).
[30] L. W. Bos, D. W. Lynch, and J. L. Stanford, Phys. Letters **30A,** 17 (1969).
[31] H. E. Bennett and J. A. Bennett, in *Physics of Thin Films*, edited by G. Hass (Academic, New York, 1967), Vol. IV, p. 1.
[32] K. G. Ramanathan, Proc. Phys. Soc. (London) **A65,** 532 (1952).
[33] A. B. Pippard, Phil. Trans. Roy. Soc. London **A250,** 325 (1957).
[34] M. A. Biondi, Phys. Rev. **102,** 964 (1956).
[35] M. A. Biondi and J. A. Rayne, Phys. Rev. **115,** 1522 (1959).
[36] M. A. Biondi and A. J. Guobadia, Phys. Rev. **166,** 667 (1968).
[37] C. Nanney, Phys. Rev. **129,** 109 (1963).
[38] L. R. Harris and R. T. McGinnies, J. Opt. Soc. Am. **38,** 582 (1948).
[39] W. R. Blevin and W. J. Brown, Metrologia **2,** 139 (1966).
[40] O. N. Carlson, F. A. Schmidt, and W. M. Paulson, Trans. Am. Soc. Met. **57,** 356 (1964).
[41] A. P. Lenham, J. Opt. Soc. Am. **57,** 473 (1967).
[42] R. W. Graves and A. P. Lenham, J. Opt. Soc. Am. **58,** 884 (1968).
[43] M. A. Lind (private communication).
[44] J. S. Toll, Phys. Rev. **104,** 1760 (1956).
[45] F. Stern, Solid State Phys. **15,** 299 (1963).
[46] P. Girault, P. Seignac, A. Priol and S. Robin, Compt. Rend. **266,** 688 (1968).
[47] R. P. Gupta and S. K. Sinha, Phys. Rev. (to be published).
[48] B. Lebech and K. Mikke, Danish Atomic Energy Commission Report No. 811, Risø, Boekilde, Denmark, 1968 (unpublished).
[49] M. Sachs, Phys. Rev. **107,** 437 (1957).
[50] G. F. Koster, Solid State Phys. **5,** 173 (1957).
[51] H. Jones, *Theory of Brillouin Zones and Electronic States in Crystals* (Interscience, New York, 1960).
[52] J. E. Graebner and J. A. Marcus, Phys. Rev. **175,** 659 (1968).
[53] B. R. Cooper, H. Ehrenreich, and H. R. Philipp, Phys. Rev. **138,** A494 (1965).